Electronic Supplementary Material (ESI) for Journal of Materials Chemistry C.

Supporting Information

A Portable Fiber Optic Sensor for the Luminescent Sensing of Cobalt Ions using Carbon Dots

Scott E. Crawford,*[a,b] Ki-Joong Kim,[a,b] and John P. Baltrus[a]

[a]National Energy Technology Laboratory, 626 Cochrans Mill Road, Pittsburgh, Pennsylvania 15236, United States.

[b]NETL Support Contractor, 626 Cochrans Mill Road, Pittsburgh, Pennsylvania 15236, United States

*E-mail: Scott.Crawford@netl.doe.gov

Table of Contents:

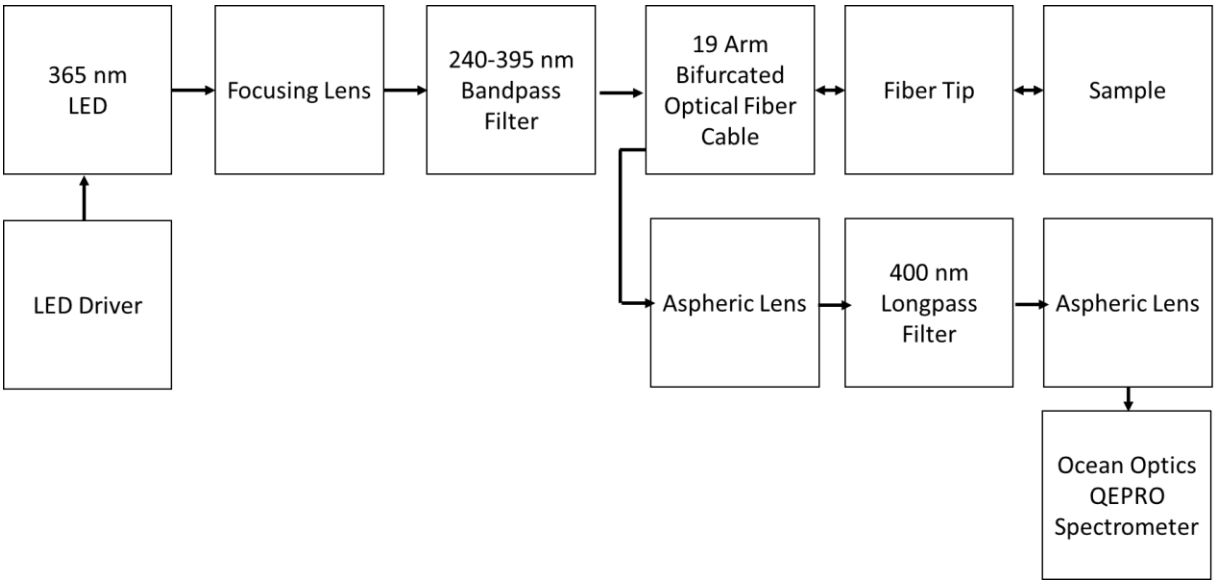

Figure S1. Schematic illustrating the portable fiber optic luminescence spectrometer used to detect cobalt ions

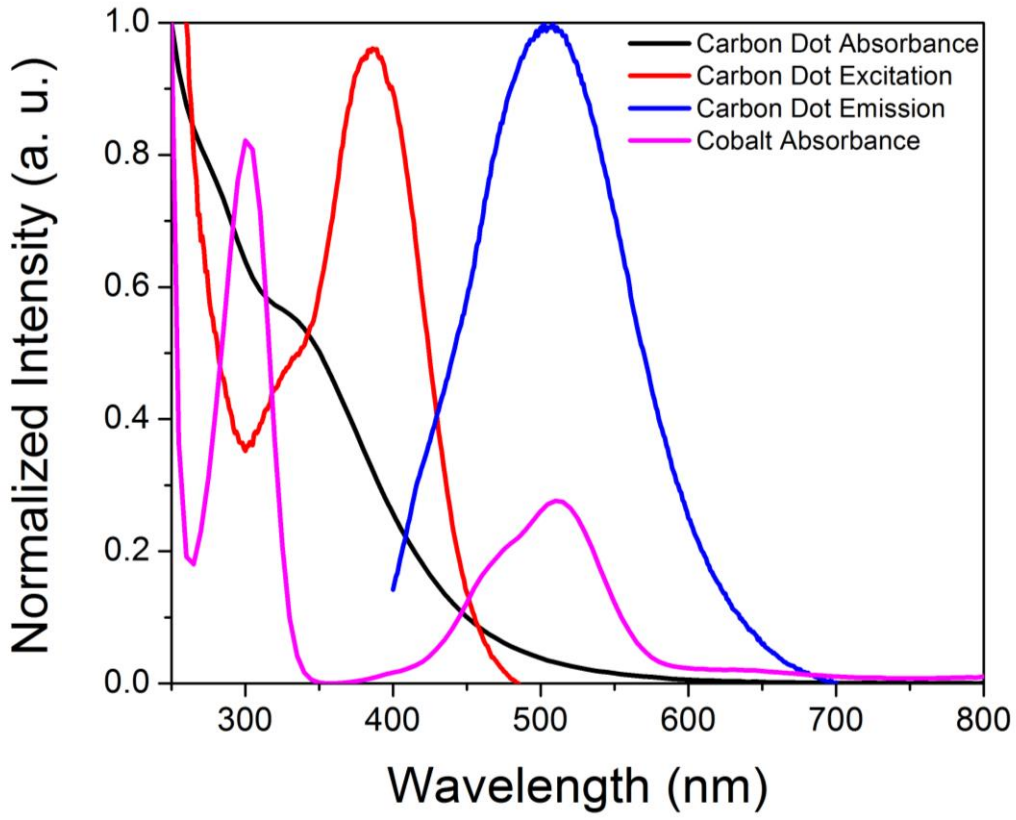

Figure S2. Normalized excitation, emission, and absorption spectra of the carbon dot sensor for cobalt, and the absorbance spectrum of 0.05 M $Co(NO_3)_2$ in water.

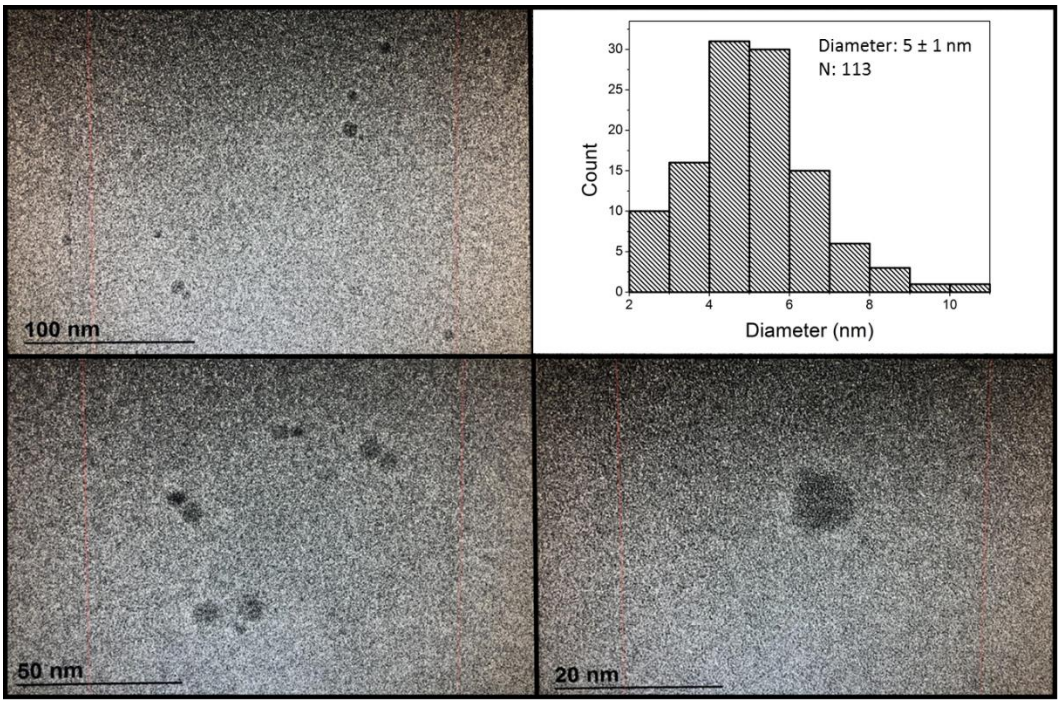

Figure S3. TEM images of the carbon dots taken at different magnifications, with a histogram of the measured diameters from over 100 nanoparticles.

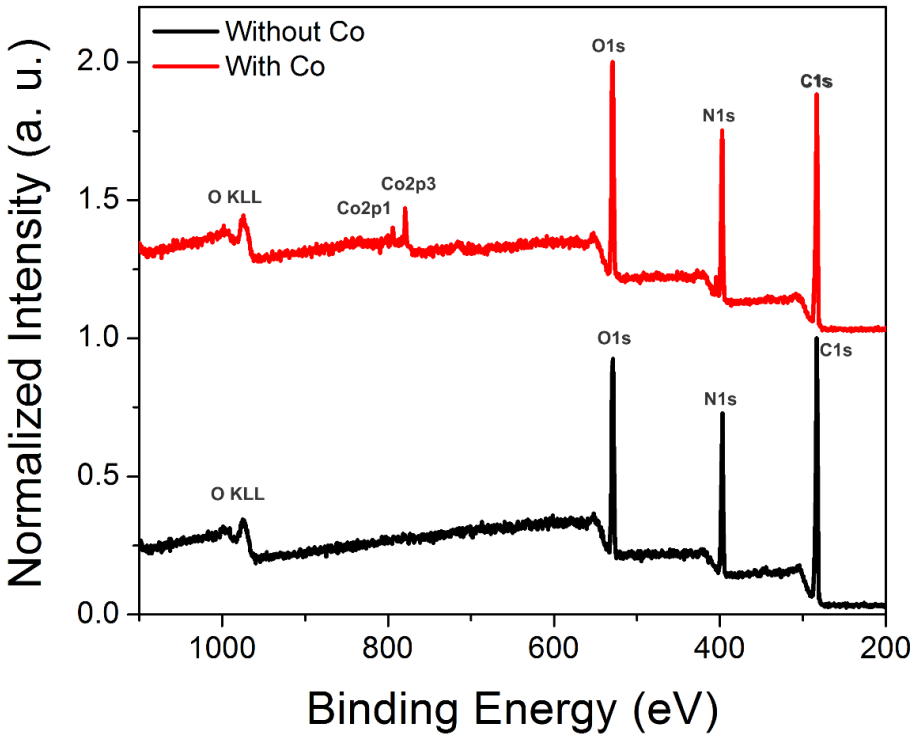

Figure S4. XPS survey spectra of carbon dots with and without cobalt exposure**.**

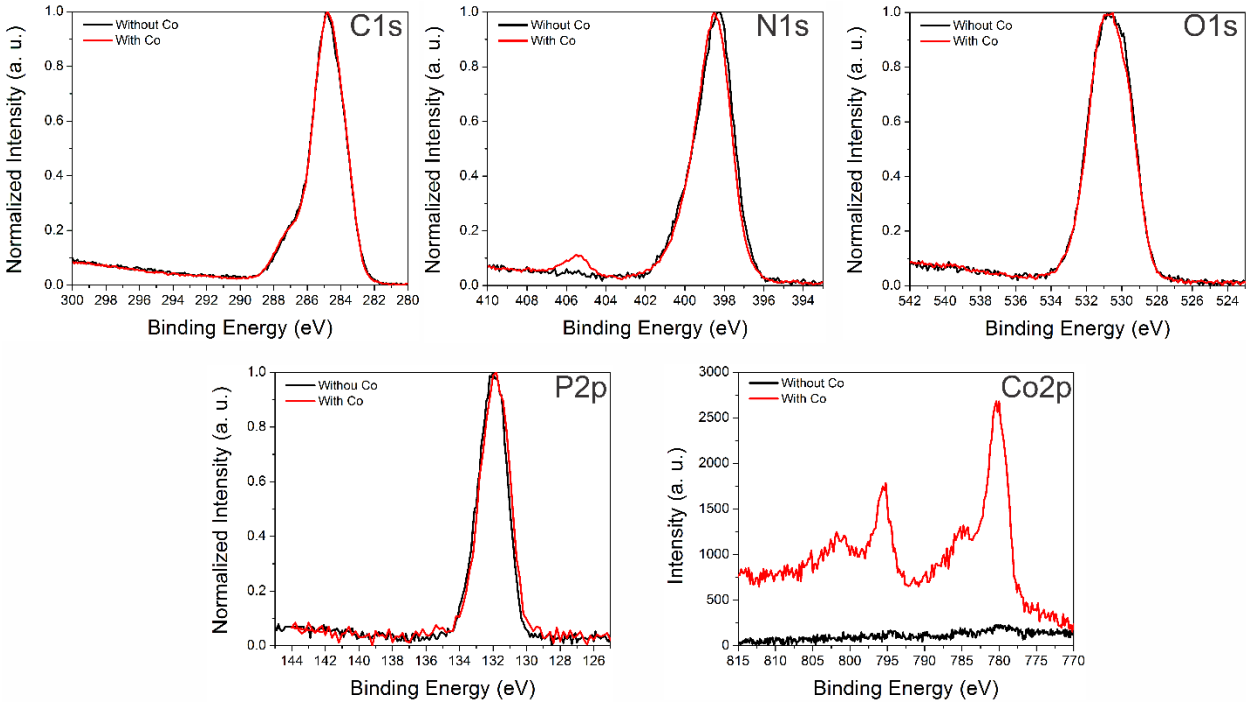

Figure S5. High resolution XPS spectra of C1s, N1s, O1s, P2p, and Co2p with and without cobalt exposure.

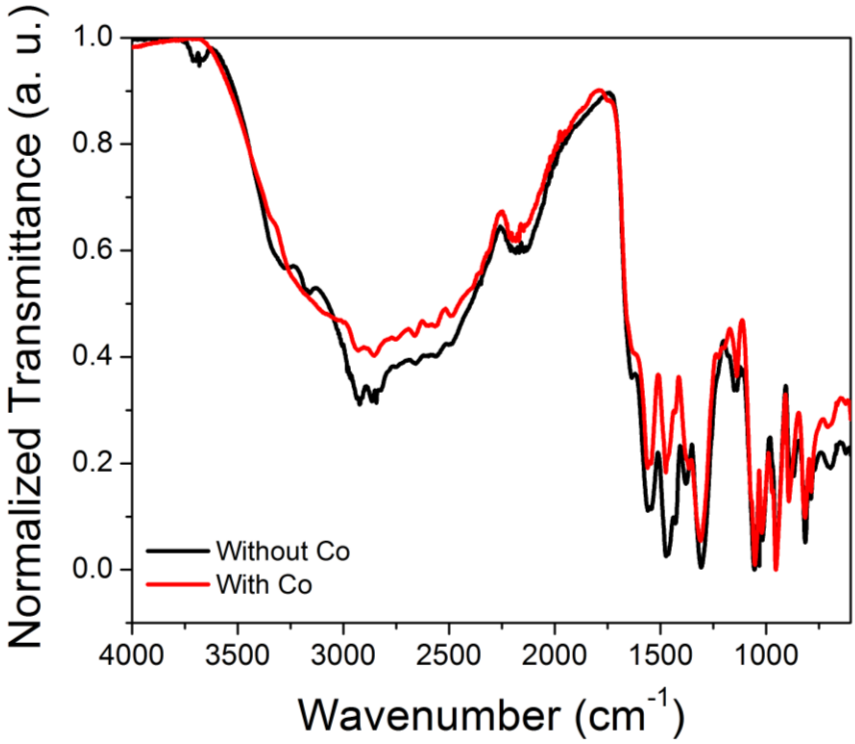

Figure S6. Fourier-Transform infrared spectra (FTIR) of the carbon dots before and after exposure to cobalt**.**

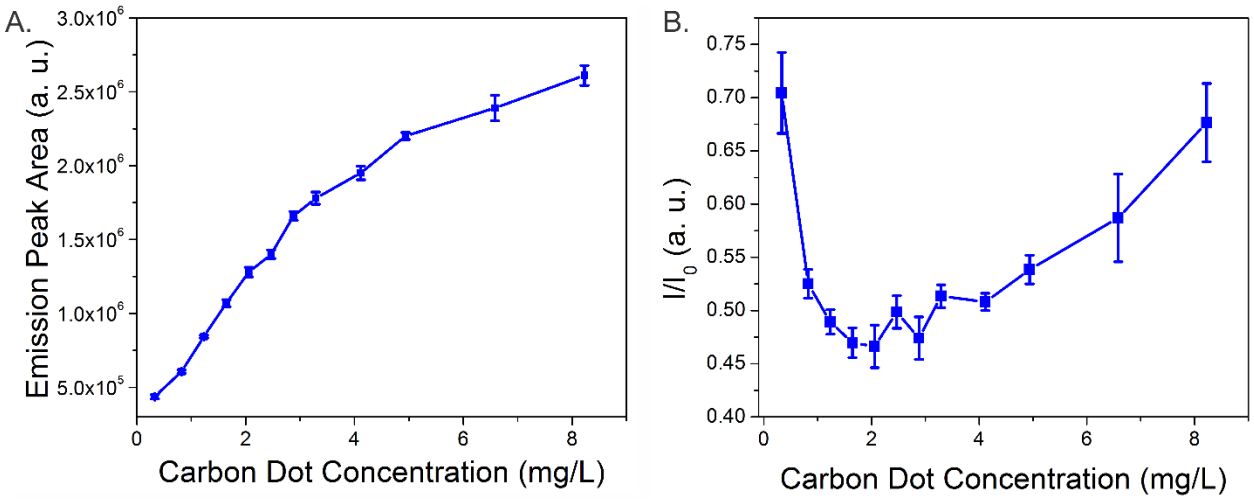

Figure S7. Impact of carbon dot concentration on emission peak intensity (A) and sensitivity to the addition of 0.5 mM cobalt (B). Error bars represent the standard error of three independent trials.

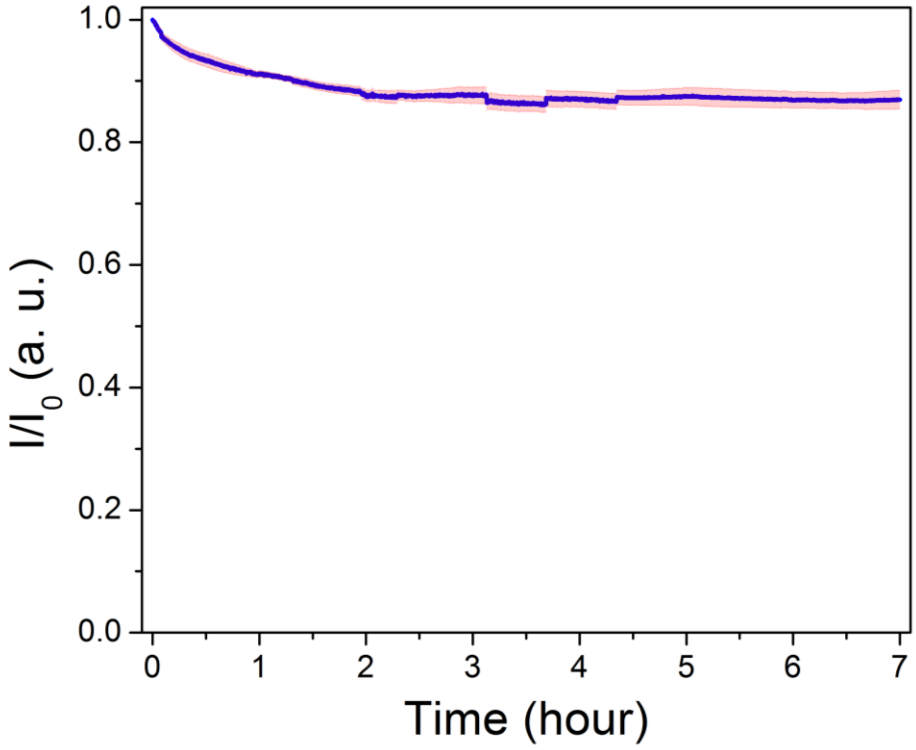

Figure S8. Intensity changes of carbon dots over time under continuous illumination of a 365 nm LED. Error bars represent the standard error of three independent trials.

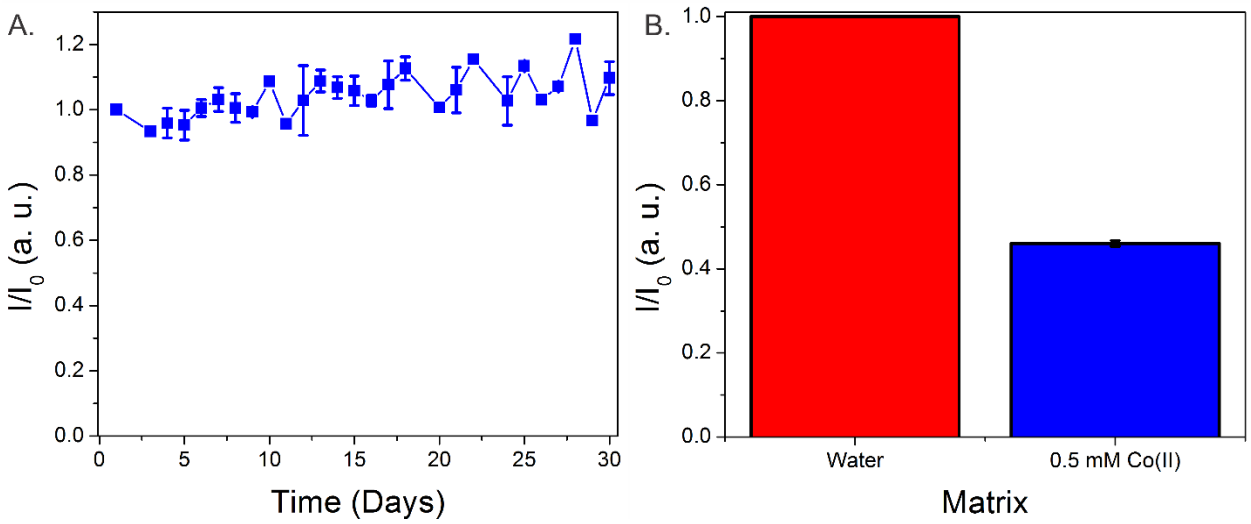

Figure S9. Intensity changes of 4 carbon dot samples measured over the course of 1 month (A). Change in intensity in response to the addition of 0.5 mM cobalt following 1 month of storage (B). Error bars denote the standard error of points containing multiple trials

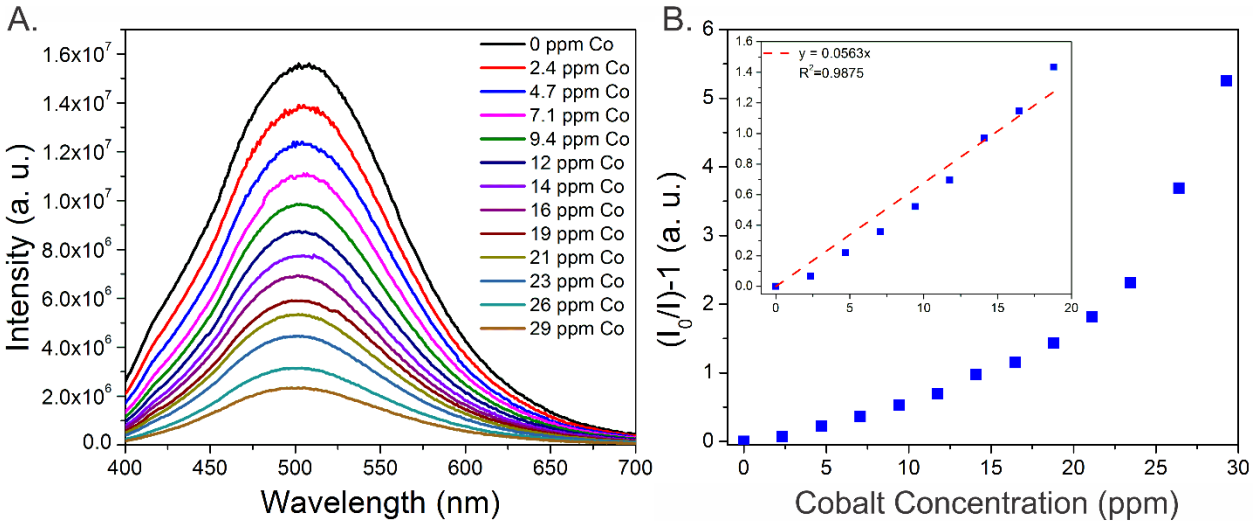

Figure S10. Emission peak of carbon dots in deionized water as a function of Co^{2+} concentration (A). Stern-Volmer profile of the emission quenching (B). INSET: Linear portion of the Stern-Volmer profile used to create a calibration curve for sensitivity estimations.

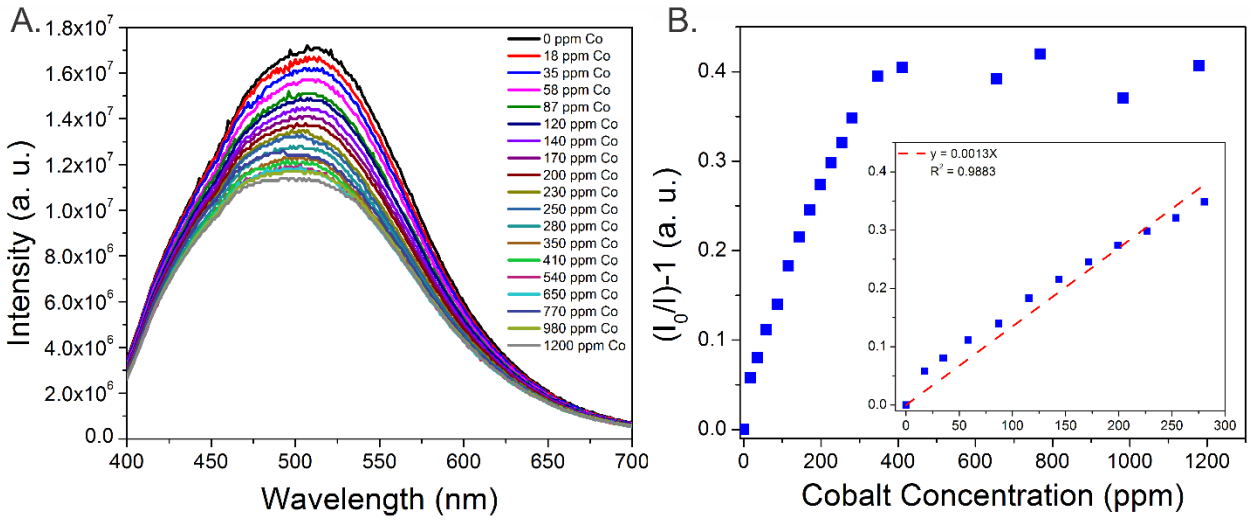

Figure S11. Emission peak of carbon dots in pH 1.68 buffer as a function of Co^{2+} concentration (A). Stern-Volmer profile of the emission quenching (B). INSET: Linear portion of the Stern-Volmer profile used to create a calibration curve for sensitivity estimations.

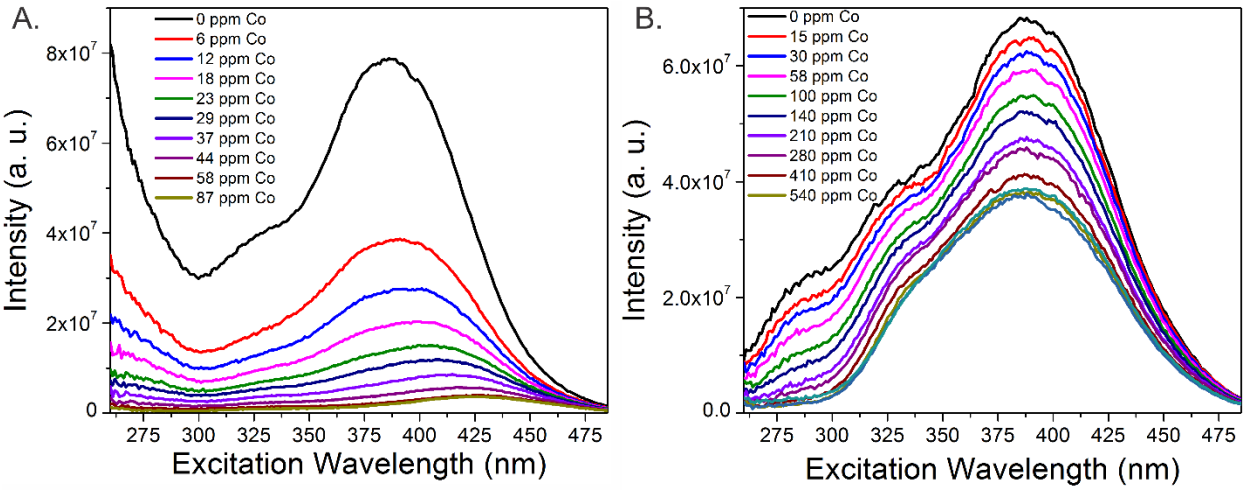

Figure S12. Excitation spectra of carbon dots as a function of cobalt concentration in deionized water (A) and pH 1.68 buffer (B)**.**

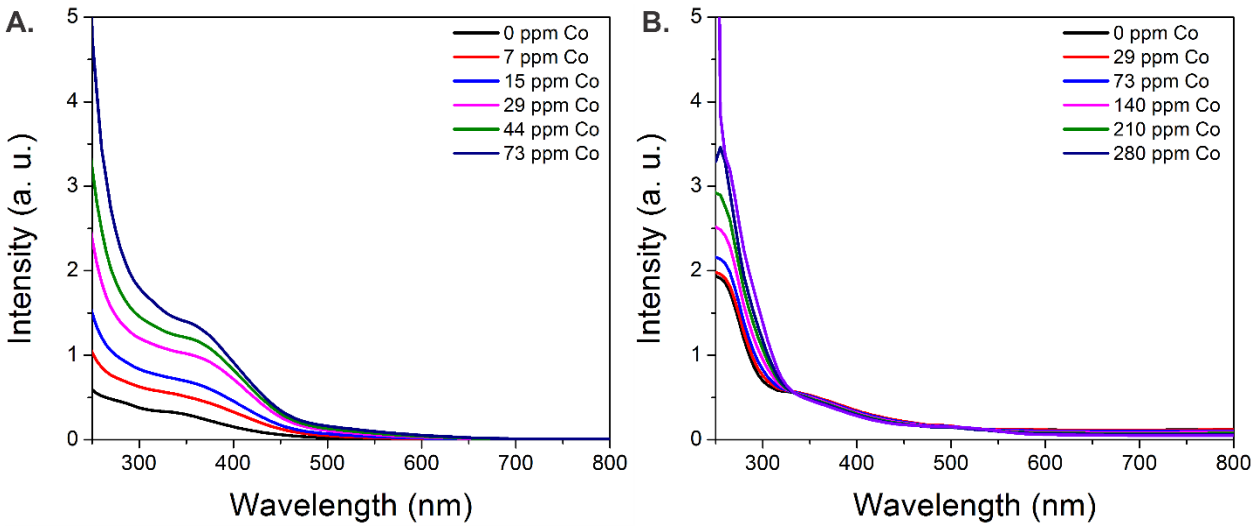

Figure S13. Absorption spectra of the carbon dot sensors as a function of increasing cobalt concentration in (A) deionized water and (B) pH 1.68 buffer.

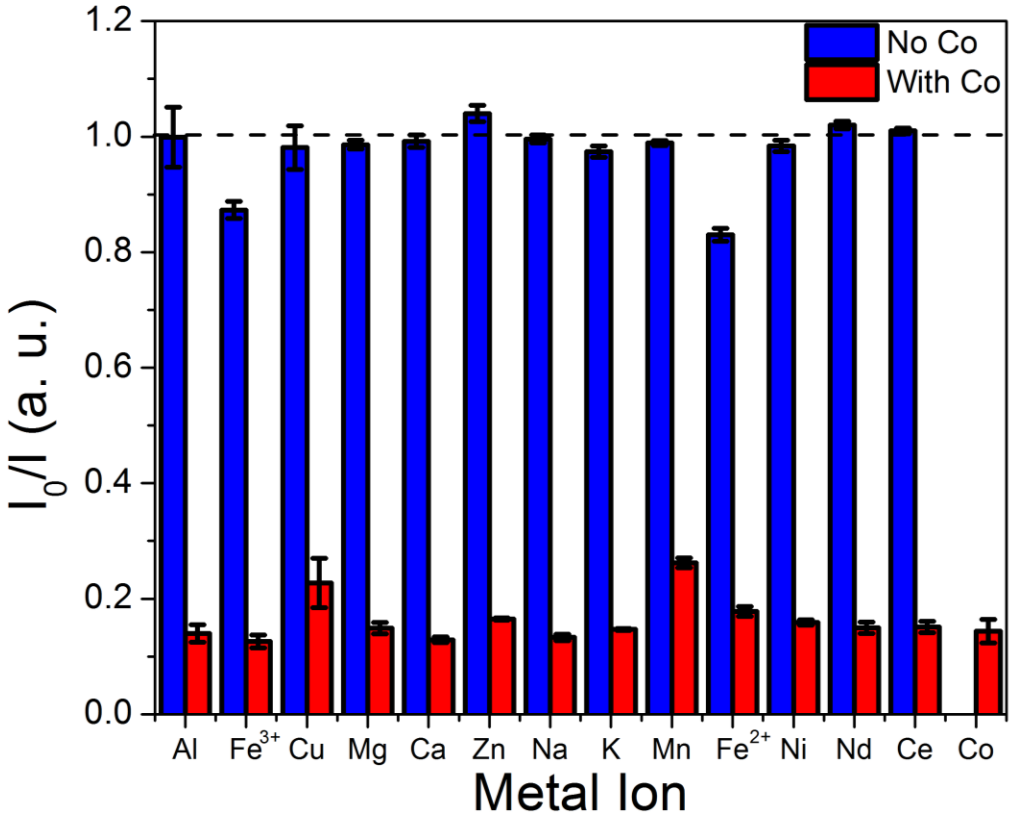

Figure S14. Changes in the carbon dot peak area after the addition of 0.5 mM of different metals (blue) and after the subsequent addition of 0.5 mM cobalt (red), recorded using the Fluorolog 3 system.

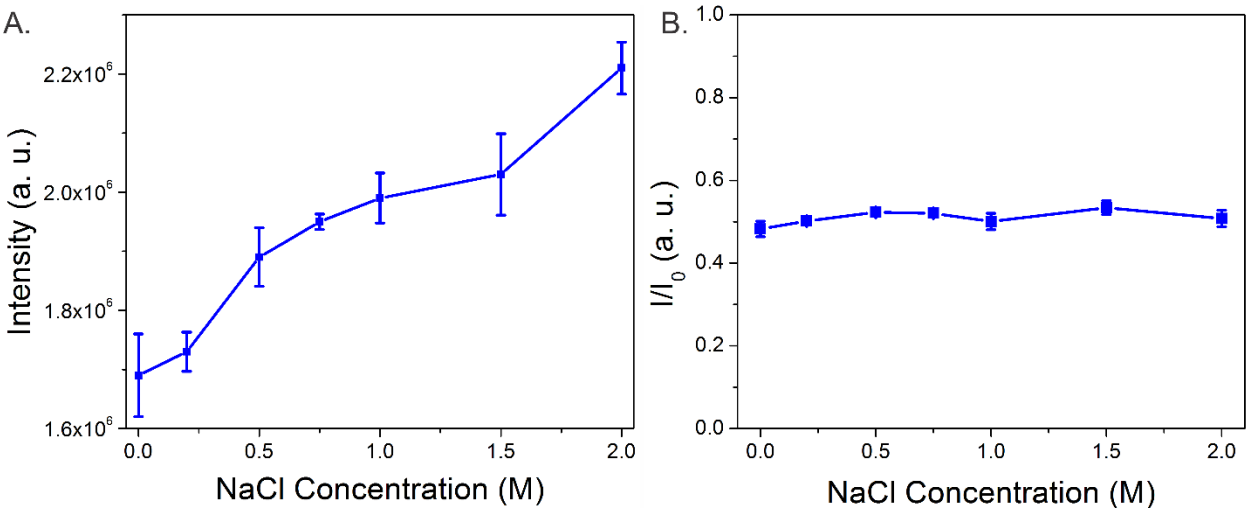

Figure S15. Impact of matrix salinity on the carbon dot emission peak intensity (A) and sensitivity to the addition of 0.5 mM cobalt (B). Error bars represent the standard error of three independent trials.

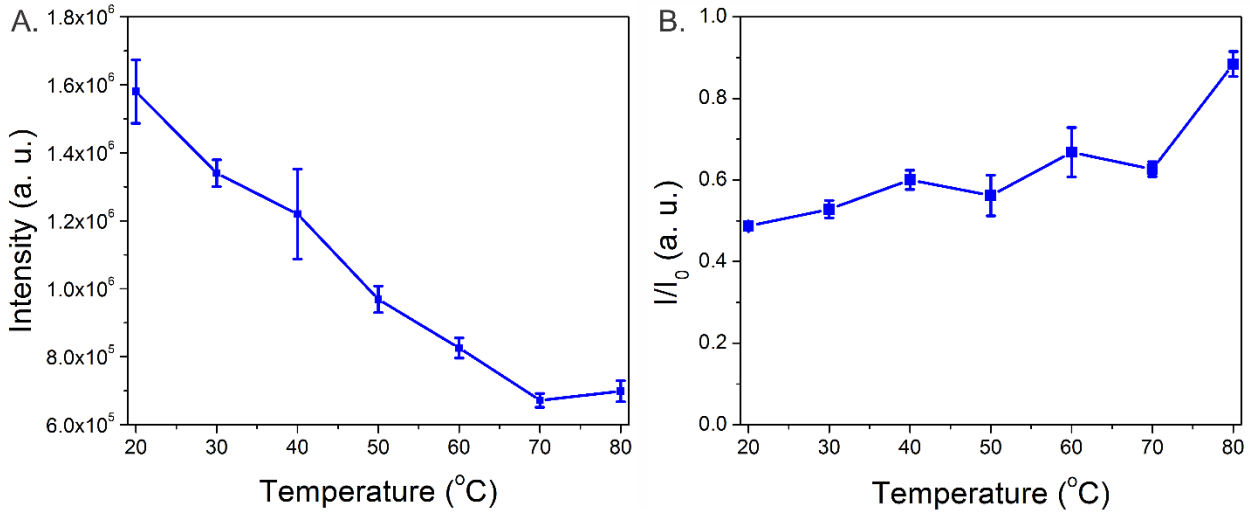

Figure S16. Impact of matrix temperature on the carbon dot emission peak intensity (A) and sensitivity to the addition of 0.5 mM cobalt (B). Error bars represent the standard error of three independent trials.

Table S1. ICP-MS Metal Concentrations of Acid Mine Drainage Leachate

Metal	Concentration (ppm)
Al	4890
Na	0.9
Mg	56
Si	2180
P	0.9
K	3.0

Ca	291
Sc	1.9
Mn	140
Fe	140
Co	5.1
Ni	37
Zn	190
Sr	1.2
Y	16
Zr	0.03
La	5.8
Ce	14
Pr	2.3
Nd	10
Sm	3.1
Eu	0.7
Gd	3.7
Tb	0.6
Dy	3.3
Ho	0.7
Er	1.80
Tm	0.2
Yb	1.4
Lu	0.2
Pb	0.002
Th	0.4
U	0.9

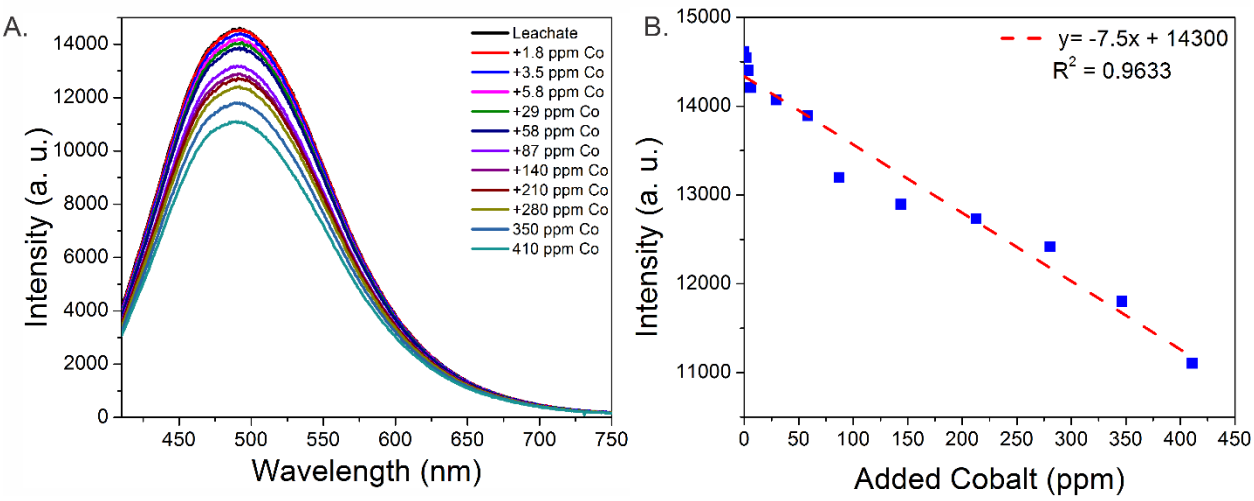

Figure S17. Emission spectra (A) and peak intensity (B) as a function of cobalt concentration added to an acid mine drainage leachate solution.

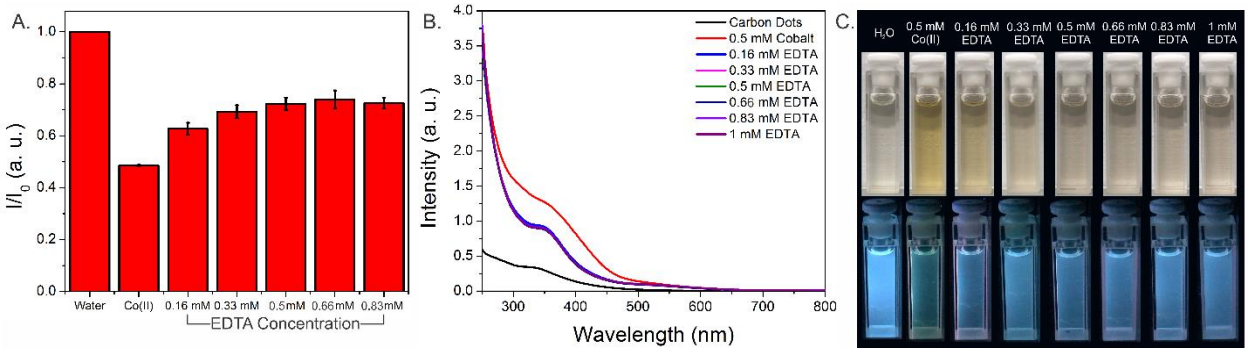

Figure S18. Changes in emission peak area of the carbon dots before and after exposure to 0.5 mM cobalt, and after the addition of increasing amounts of the chelating agent EDTA, which partially restores emission (A). Changes in the absorption of the carbon dots before and after exposure to 0.5 mM cobalt, and after the addition of increasing amounts of the chelating agent EDTA, which leads to reduced absorbance in the UV (B). Optical photographs of a dilute carbon dot solution exposed to cobalt and then subsequent additions of EDTA under ambient and UV light (C).

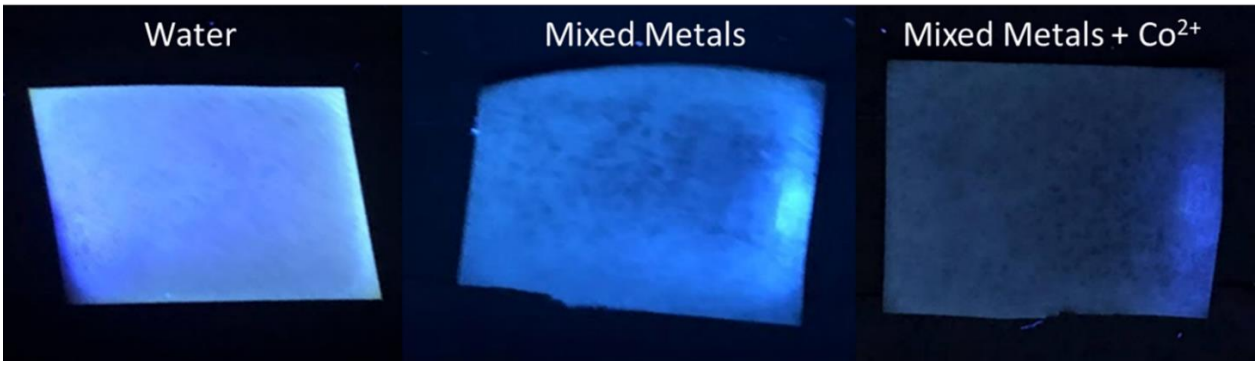

Figure S19. Photograph of carbon-dot coated filter paper strips under UV light after exposure to water, a mixed metal solution (10 mM each of Al(III), Fe(II), Fe(III), Na(I), K(I), Ni(II), Cu(II), Mg(II), Mn(II), Ca(II), Ce(III), Nd(III), and Zn(II)), and the mixed metals with 10 mM Co(II) also present.

Table S2. ICP-MS Characterization of the Acid Mine Drainage Matrix (pH: 3.3)

Analyte	Concentration (ppm)
Li	0.118
Na	15.1
Mg	29.33
Al	9.84
Si	12.56
P	<DL*
K	0.946
Ca	59.25
Sc	0.00165
Ti	0.001
V	<DL*
Cr	0.00206
Fe	0.32
Co	0.0408
Ni	0.108
Cu	0.0122

Zn	1.29
As	<DL*
Se	<DL*
Sr	0.81
Y	0.0144
Zr	0.000153
Cd	0.00124
Ba	0.881
La	0.00674
Ce	0.0239
Pr	0.00372
Nd	0.0173
Sm	0.00472
Eu	0.00123
Gd	0.00483
Tb	0.000722
Dy	0.00338
Ho	0.000587
Er	0.00151
Tm	0.000185
Yb	0.00102
Lu	0.000139
Pb	<DL*
Th	<DL*
U	<DL*

*<DL indicates that the elemental concentration is below the ICP-MS detection limit

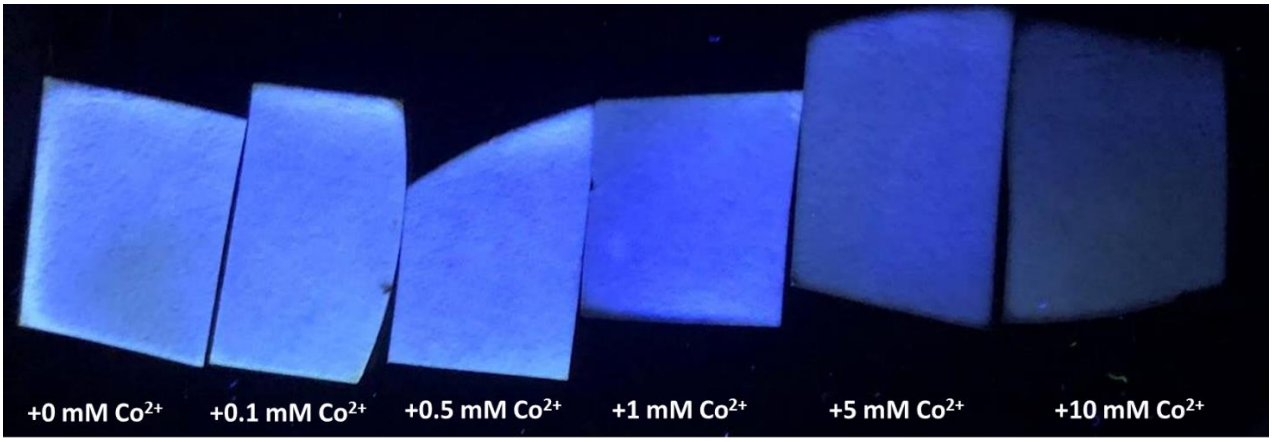

Figure S20. Photograph of carbon-dot coated filter paper strips under UV light after exposure to pure acid mine drainage, and acid mine drainage spiked with different cobalt concentrations. Despite the low pH and presence of other metals, the emission is quenched at increasing cobalt concentrations.